Optical, Electrical, and Magnetic Studies of Organic Solar Cells Based on Low Bandgap Copolymer with Spin ½ Radical Additives

*Tek Basel, Uyen Huynh, Tianyue Zheng, Tao Xu, Luping Yu, and Z. Valy Vardeny**

The charge photogeneration and recombination processes in organic photovoltaic solar cells based on blend of the low bandgap copolymer, PTB7 (fluorinated poly-thienothiophene-benzodithiophene) with C60-PCBM using optical, electrical, and magnetic measurements in thin films and devices is studied. A variety of steady state optical and magneto-optical techniques were employed, such as photoinduced absorption (PA), magneto-PA, doping-induced absorption, and PA-detected magnetic resonance (PADMR); as well as picosecond time-resolved PA. The charge polarons and triplet exciton dynamics in films of pristine PTB7, PTB7/fullerene donor–acceptor (D–A) blend is followed. It is found that a major loss mechanism that limits the power conversion efficiency (PCE) of PTB7-based solar cell devices is the "back reaction" that leads to triplet exciton formation in the polymer donor from the photogenerated charge-transfer excitons at the D–A interfaces. A method of suppressing this "back reaction" by adding spin½ radicals Galvinoxyl to the D–A blend is presented; this enhances the cell PCE by ≈30%. The same method is not effective for cells based on PTB7/C70-PCBM blend, where high PCE is reached even without Galvinoxyl radical additives.

1. Introduction

Organic photovoltaic (OPV) is an emerging field that has seen a rapid development in recent years driven by the low cost, flexible device structure, and easy fabrication processes.[1–13] In response to the low power conversion efficiency (PCE) of OPV based on bilayer device structure[1] in which, donor (D) and acceptor (A) layers are deposited sequentially, the OPV research field has moved to devices based on bulk heterojunction (BHJ) structure from donor–acceptor (D–A) blends,[8,11,14,15] where bicontinuous interpenetrating network of separated donor and acceptor domains are formed. BHJ photovoltaic cells maximize photon absorption and allows photogenerated singlet excitons in the donor domain to reach the D–A interfaces before they recombine.[5,7] Although there has been a significant increase in PCE of devices based on BHJ using the chemical synthesis versatility of the organic active layer,[9,10,16,17] the OPV field has not yet reached practical applications. There has been significant progress in the synthesis of new organic donors for harvesting the near-infrared solar illumination spectrum using low bandgap (LBG) copolymers,[17,18] optimizing the donor/acceptor ratio, the organic active layer thickness,[19] using suitable transport layers, and the device electrodes,[2,20] improving morphology,[21] and employing a tandem cell architecture.[3,22] Compared with the ≈5% PCE[23] reported for most studied cells based on polymer/fullerene blends such as regio-regular poly(3-hexylthiophene) (P3HT)/1-(3-(methoxycarbonyl)propyl)-1-phenyl)(6,6) C_{61} (C60-PCBM), PCE of 10.6% in tandem OPV cell based on LBG copolymers has been recently reported.[3] However, one problem that has prevented reaching even higher PCE in OPV cells based on the new copolymers is that the complex mechanism of charge photogeneration at the D–A interfaces in the D–A blend is still not fully understood.

The ideal polymer solar cell having a BHJ structure should exhibit the following set of physical properties: a broad absorption spectrum with high absorption coefficient that matches the solar illumination spectrum; a bicontinuous network with D–A domain size of the order of the exciton diffusion length in the polymer donors; and large D–A interfacial area that favors exciton dissociation and efficient transport of separated charges to the respective electrodes.[24] Upon solar light absorption by the polymer donor, singlet excitons are formed, diffuse to the D–A interfaces, and may subsequently dissociate[25] leading to long-range charge separation or formation of bound interfacial charge-transfer state (CT).[16,26,27] The CT state, initially in a singlet spin configuration (^{1}CT), may undergo intersystem crossing to the triplet spin configuration,^{3}CT; recombine to the ground state; or separate into Coulombically bound polaron pairs (PP) having a relatively long lifetime. The PP species may dissociate at later time and consequently generate free carriers that are collected at the electrodes producing current in the external circuit; or recombine to the ground state leading to recombination loss. During the PP or free carrier recombination processes, large density of ^{3}CT (statistically 3:1 ratio of ^{3}CT to ^{1}CT population) may be also formed. If the ^{3}CT state is at

Dr. T. Basel, U. Huynh, Prof. Z. V. Vardeny
Department of Physics & Astronomy
University of Utah
Salt Lake City, UT 84112, USA
E-mail: val@physics.utah.edu
T. Zheng, Dr. T. Xu, Prof. L. Yu
Department of Chemistry and James Franck Institute
The University of Chicago
Chicago, IL 60637, USA

DOI: 10.1002/adfm.201403191

higher energy, than the polymer lowest triplet state (T_1) [namely E(^{3}CT))>E(T_1)], which is usually the case in D–A blends of LBG copolymers,[28] and the ^{3}CT dissociation rate is small, then energy transfer from ^{3}CT to T_1 in the copolymer chains may occur.[25] This process has been recognized as one of the major losses in LBG cells performance, and thus several methods have been employed to eliminate this loss. However, the process of reducing the ^{3}CT state density by spin manipulation has been largely ignored so far.

In this work, we demonstrate a method for minimizing the loss channel via triplet excitons (TEs) in the copolymer donors in OPV cells. Previously, we reported PCE enhancement in P3HT/PCBM-based OPV devices by ≈18% when adding to the D–A blend spin½ radicals, galvinoxyl (2,6-di-*t*-butyl-α-(3,5-di-*t*-butyl-4-oxo-2,5-cyclohexadien-1-ylidene)-*p*-tolyloxy) [Gxl].[19] Here, we report on another D–A blend, namely PTB7/C60-PCBM that shows superior OPV performance upon adding Gxl spin ½ radicals. PTB7 is a LBG copolymer of which, repeat unit contains alternating fluorinated thienothiophene (FTT) and benzodithiophene blocks (molecular structure shown in **Figure 1**b), that yields high PCE of >7% in OPV cells.[7] Because of the electron affinity difference between the alternating intrachain blocks, these new copolymers show broad absorption spectrum band in both the UV–vis and near-IR regions.[29]

Through continuous wave (cw) and transient optical experiments, and magnetic and electrical studies of pristine PTB7 copolymer films and its blend with C60-PCBM, we identified that the spin ½ Gxl radical additives in the blends facilitate CT intersystem conversion from triplet to singlet (^{3}CT→^{1}CT), which consequently enhances the charge separation leading to increased short-circuit photocurrent density (J_{sc}) in OPV devices based on this blend. This is supported by optical measurements that show a reduction in the TE density in the copolymer donors. In our studies, we employed the techniques of photoinduced absorption (PA), magneto-PA (MPA), and PA-detected magnetic resonance (PADMR) to identify and monitor the TEs in the copolymer donors. We also used the ps time resolved PA to verify the underlying processes. As a control experiment, we compared our results in PTB7/C60-PCBM to those in PTB7/C70-PCBM, where Gxl has detrimental effect on the cell performance, which does not show a reduction of the polymer TE density.

2. Results and Discussion

Figure 1a shows the absorption and PL spectra of pristine PTB7 copolymer. The absorption band is red-shifted compared with more traditional π-conjugated polymers such as P3HT and PPV, which fits better the sun illumination spectrum. The copolymer has an absorption band that peaks at 1.8 eV having a phonon side band at ≈2 eV; whereas the absorption onset is at ≈1.7 eV, which determines the optical gap. The PL spectrum has a 0–0 line at ≈1.55 eV and 0–1 vibronic replica at 1.38 eV. The PL quantum efficiency of this polymer was measured to be an impressive is 24%, which is comparable to that of the best π-conjugated polymers. This indicates well-separated polymer chains that suppress aggregation.

To understand the carrier photogeneration process, we studied the photophysics of thin films of pristine PTB7 in comparison with that of PTB7/C60-PCBM blend. In **Figure 2**a, we show the cw PA spectrum of pristine PTB7 at 45 K. The spectrum shows a dominant PA band at 1.1 eV, and there are no other PA bands at lower photon energy. To identify the polaron and TE PA bands in the spectrum, we performed three crucial measurements. First, the doping-induced absorption

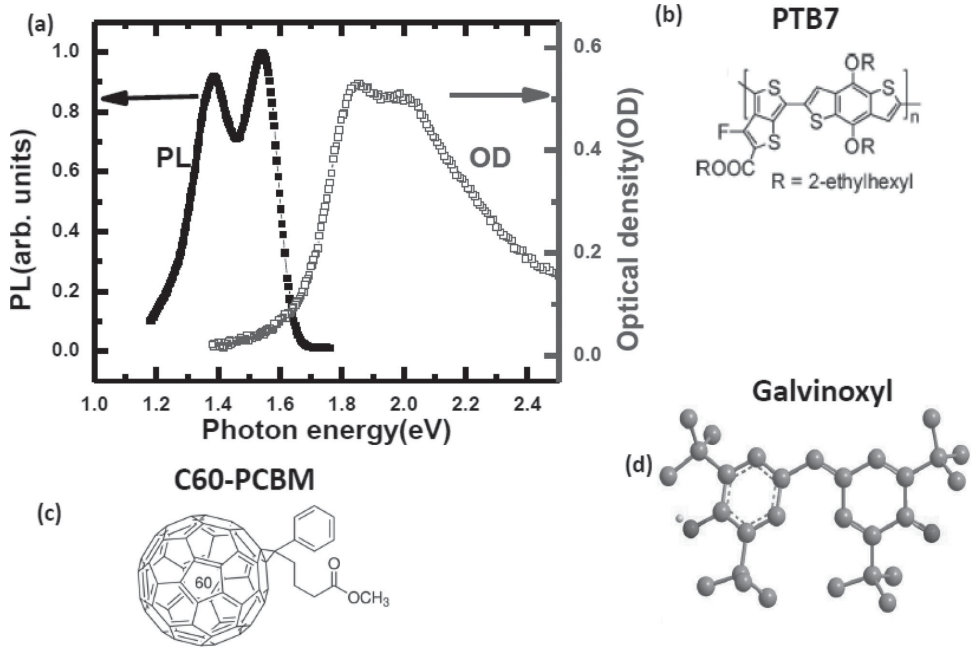

Figure 1. a) Absorption (open squares) and PL (filled squares) spectra of pristine PTB7 copolymer. The molecular structures are shown in b) PTB7; c) C60-PCBM; and d) Galvinoxyl spin ½ radical.

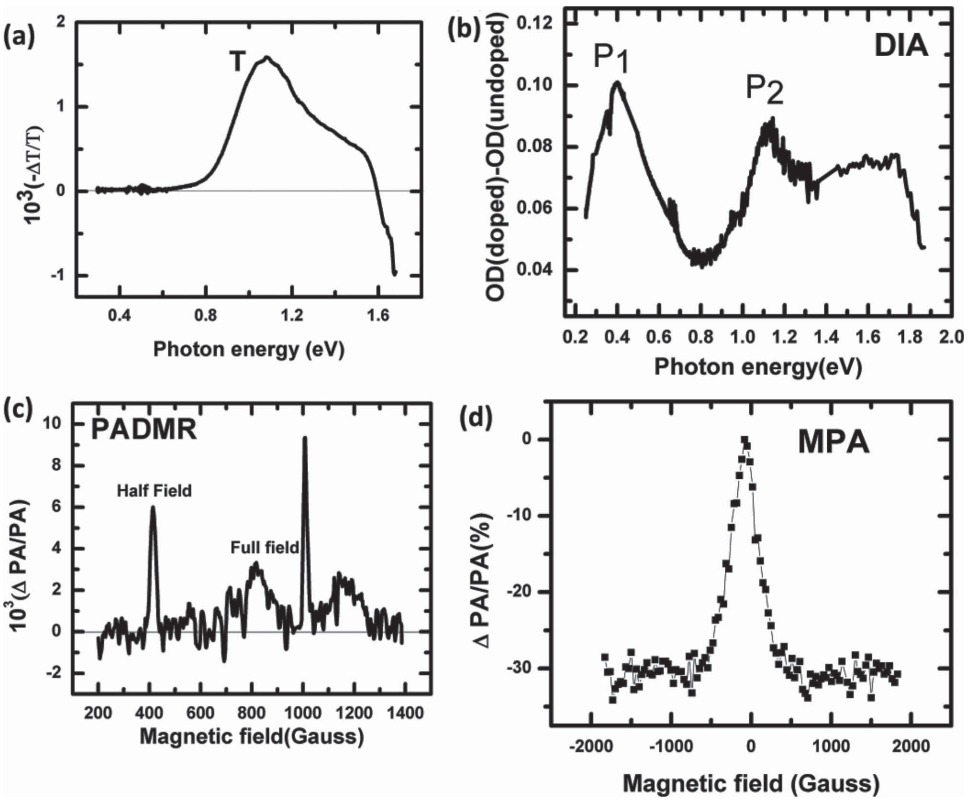

Figure 2. Photophysics of pristine PTB7 copolymer. a) PA spectrum. b) DIA spectrum of the PTB7 film exposed to Iodine vapor for 1 min at room temperature. The two polaron DIA bands P_1 and P_2 are denoted. c) PADMR of PTB7 polymer at probe energy 1.1 eV. The triplet full field and half-field powder patterns, and spin ½ resonance are denoted. d) MPA(*B*) response measured at 1.1 eV that originates from TEs.

(DIA) technique is used to identify the charge species in the PTB7 chains. For this, we exposed the pristine copolymer film with iodine vapor for 1 min, and the difference in the absorption spectra before and after iodine doping was measured. The DIA spectrum in Figure 2b shows DIA bands at 0.4 and 1.1 eV, respectively. These two bands are assigned to P_1 and P_2 polaron bands that are related to two formed in-gap states in the π-conjugated copolymer chain.[30,31] Second, we performed PADMR measurements to identify the spin multiplicity of the photoexcitations associated with the PA band in this copolymer. Figure 2c shows the PADMR(*B*) spectrum of the dominant PA band in the spectrum; it shows both full field (FF, around ≈1000 G) and half field (HF≈400 G) powder pattern resonances. These resonance bands are formed from transitions between three different spin energy sublevels of S = 1 species. We also performed magnetic-PA (MPA) at 1.1 eV as shown in Figure 2d. The MPA(*B*) response is much broader than the hyperfine interaction in π-conjugated polymers (≈30 Gauss), and therefore it originates from much stronger interaction.[32] Such interaction is formed in the spin sublevels of TE due to dipolar interaction between the electron and hole, which is dubbed zero-field splitting (ZFS) having typical ZFS parameter, D. From the saturation field of the MPA(*B*) response, we obtain D≈550 G. This is in good agreement with D≈560 G obtained from the FF powder pattern in the PADMR(*B*) spectrum (Figure 2c).[33]

Equipped with these three measurements, we can now identify the dominant PA band in the pristine PTB7. Since the PA spectrum shows a single band at 1.1 eV, it cannot originate from polaron excitations, which would show another band at ≈ 0.4 eV. This indicates that the polymer has very good quality, since polaron photogeneration in pristine π-conjugated polymers is usually related to the existence of defects and/or impurities in the polymer film.[34] In addition, from the PADMR spectrum at 1.1 eV, we know that the spin **state** associated with this band **is triplet.** We therefore identify the PA band as due to long-lived S = 1 TE in the PTB7 chains.

In contrast to the PA spectrum of pristine PTB7, the PA spectrum of the PTB7/C60-PCBM blend shows two PA bands at 0.4 and 1.1 eV, respectively (**Figure 3**a); but the PA at 1.1 eV is much stronger. From the PA and DIA spectra of pristine PTB7, we conclude that the PA band at 0.4 eV is due to the P_1 transition associated with photogenerated polarons, whereas the PA band at 1.1 eV has contributions from both TE (T) and polarons (P_2). However, judging from the weak P_1 band in the PA spectrum, we conclude that the TE contribution to the PA at 1.1 eV is much stronger than that of P_2. This is also supported by the MPA(*B*) response at 1.1 eV (Figure 3b), which is similar to that of the MPA(*B*) response in pristine PTB7 (Figure 2d). This shows that substantial photogenerated TE density still exists in PTB7/C60-PCBM blend; this is a photocarrier loss mechanism in PTB7/C60-PCBM that limits the photocurrent density in OPV cells based on this blend. The increased TE density in the blend is achieved from the "back reaction" $^3CT \rightarrow TE$ (Figure 3c), which is possible in this blend because $E(TE) < E(^3CT)$.[25] Figure 3c

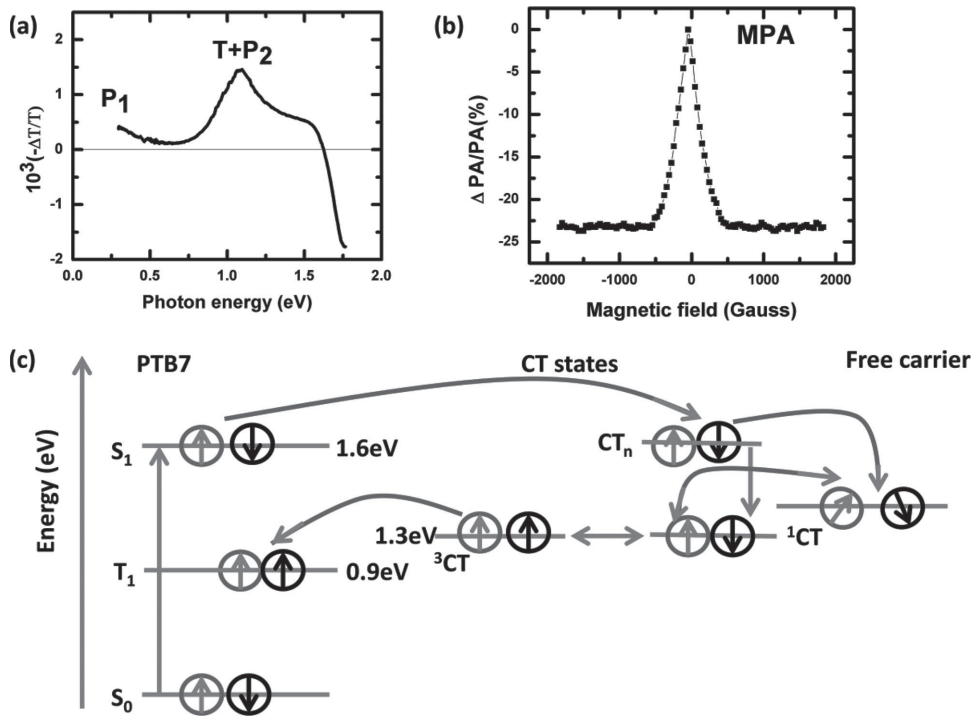

Figure 3. Photophysics and charge generation mechanism in PTB7/C60-PCBM blend. a) PA spectrum, where the PA bands P_1 and P_2+T are denoted. b) MPA(*B*) response at 1.1 eV, which originates from TE. c) Schematics of the photogeneration processes in the BHJ. Adapted with permission.[25] Copyright 2013, Nature Publishing Group.

schematically shows the process leading to excess TE in the copolymer. After singlet excitons dissociate into ^{1}CT and ^{1}PP species at the D–A interfaces, there can be two possibilities. Either the CT (PP) dissociate into free carriers that contribute to the photocurrent, or intersystem crossing occurs in the CT manifold (^{1}CT→^{3}CT), where ^{3}CT undergoes energy transfer into the TE manifold, ending in the lowest TE level T_1.

The PA spectrum of the PTB7/C60-PCBM blend doped with 2% Gxl additives is shown in **Figure 4**a. It is clearly seen that the polaron P_1 band at 0.4 eV substantially increases relative to the PA at 1.1 eV; the PA band at 1.1 eV dramatically narrows and another PA shoulder develops at ≈1.5 eV. In addition the MPA(*B*) response at 1.1 eV (Figure 4b) substantially narrows and does not resemble any longer to the MPA(*B*) response of TE (Figure 3b). All these changes show that the TE band diminishes by adding Gxl radicals to the PTB7/C60-PCBM blend. This can be also seen in Figure 4c, where we plot the intensity ratio, *r* of P_1 at 0.4 eV and the PA at 1.1 eV in the PA spectra versus the Gxl concentration. The ratio, *r* increases with the percentage Gxl and reaches saturation at ≈2%. This shows that at 2%, Galvinoxyl in the blend, the TE in the copolymer donors has vanished, and therefore additional radical additives may decrease the carrier mobility due to carrier scattering without any benefit in additional reduction of the TE density in the copolymer.

The decrease of the back reaction ^{3}CT→TE upon adding the Gxl radicals is also seen in the ps transient PA(*t*) measured at 1.1 eV (Figure 4d). In the "undoped" PTB7/C60-PCBM blend, the PA of the TE at 1.1 eV increases substantially up to ≈700 ps, showing that TE excitons are formed at a later time following CT generation at the D–A blend. However, this back reaction decreases substantially upon Gxl additives, in agreement with our steady state optical studies.

We show in **Figure 5**, a possible model for explaining the underlying mechanism of decreasing the reaction ^{3}CT→TE, and consequently increasing the charge photogeneration in PTB7/C60-PCBM blend by the radical additives; this is a modified version of Figure 3c.[25] First, photoexcited singlet excitons are transferred to charge transfer states, where they either dissociate into polarons or relax to the lowest CT state. CT excitons either dissociate to free carriers or relax to form TE, since the CT state's energy level, ≈1.27 eV, is higher than that of T_1, ≈0.9 eV in the copolymer blend.[28] We propose that the spin½ additives facilitate the intersystem conversion between ^{1}CT and ^{3}CT, and thereby suppress the CT→TE reaction. If the singly occupied energy level (SOMO) of the radical is in resonance with the CT state energy level (as depicted in Figure 5), then the intersystem conversion rate would increase due to spin–spin interaction between the spin ½ radical and ^{3}CT. Whether this interconversion increases the ^{1}CT or ^{3}CT density may depend upon recombination and dissociation rates of these states. In PTB7/C60-PCBM, we have shown that the TE in the donors is reduced when adding Gxl, implying that the radical reduces the ^{3}CT density. Next, we show that the suppression of the CT→TE back reaction has a dramatic influence over the OPV devices based on the PTB7/C60-PCBM blend.

We studied the PTB7/C60-PCBM-based OPV cell performance upon adding spin ½ radicals. In our previous work,[19] we showed that PCE of P3HT/PCBM cells increases upon adding Gxl in the blend. As seen in **Figure 6**a, the device performance substantially increases with Gxl addition. Both J_{sc} and

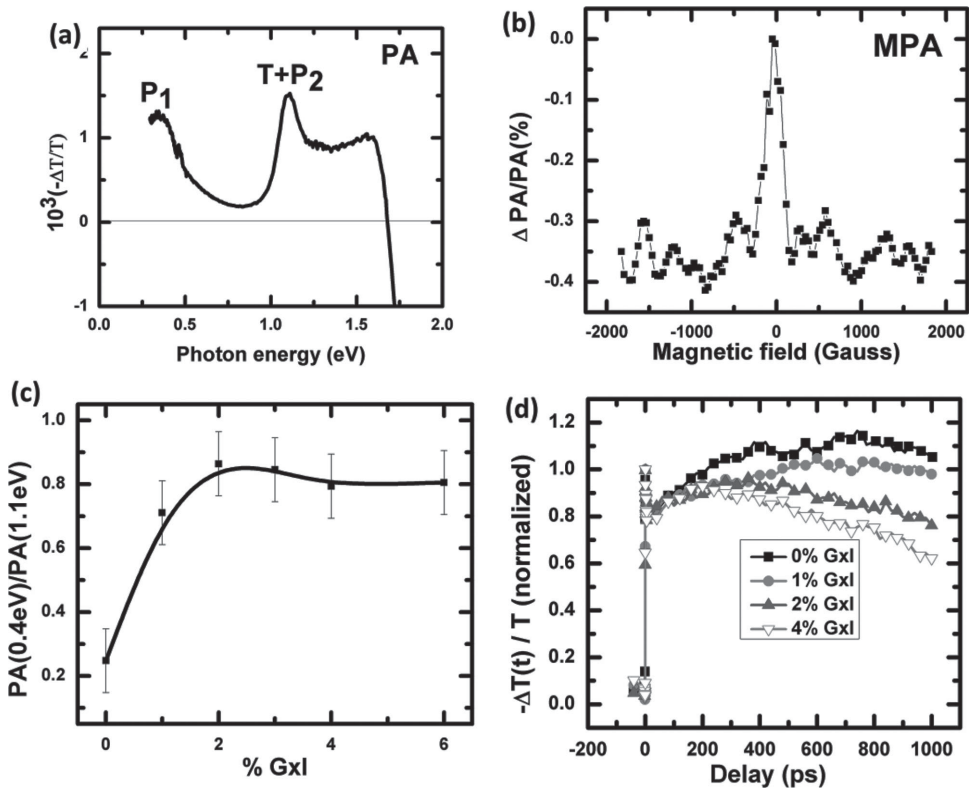

Figure 4. Photophysics of PTB7/C60-PCBM blend with GxI radical additives. a) The PA spectrum, where the PA bands P_1 and P_2 of polarons and T of TE are denoted. b) MPA(*B*) response at 1.1 eV that originates mainly from polarons. c) The ratio, *r* of the PA intensity at 0.4 (P_1) eV to that at 1.1 eV ($T+P_2$). d) ps transient PA(*t*) dynamics measured using the pump-probe correlation at 1.1 eV, obtained for various percentages weight of GxI additives.

PCE substantially increase at 2% GxI concentration (Figure 6b); however, upon adding additional GxI, actually the device performance deteriorates. The OPV device parameters J_{sc}, V_{oc}, fill factor, and PCE for various GxI percentages are listed in **Table 1**. We note that PCE increases from 5.2% to 6.8% at 2% GxI (Figure 6b), which amounts to a ≈30% increase in device performance. Figure 6b also shows that the enhancement in the device PCE is due to the increase in J_{sc} (from 10.4 mA cm^{-2} to 14.4 mA cm^{-2}) indicating that the GxI radicals enhance the photogeneration current. This can be understood as GxI-related enhancement of singlet exciton dissociation at the D–A interfaces, or reduction of the CT recombination, or both. As discussed above, one of the loss CT channel is reduced by adding GxI radicals, and this explains the photocurrent increase.

Recent morphological studies[10,35–41] in PTB7/PCBM blend shows that the small amount of the solvent additive DIO improves the morphology; thereby, dramatically increases the OPV cell performance based on blends prepared from Chlorobenzene solution. In this case, the donor and acceptor grains size decreases, and the fine miscibility of the PTB7 copolymer with fullerene results in more efficient singlet exciton dissociation at the D–A interfaces. Also, excitons' recombination is reduced upon adding DIO molecules as discussed in a previous study.[40] We have performed a series of control measurements, such as XRD (Figure S4, Supporting Information), AFM, SEM, absorption, PL, and EQE (as shown in Figures S1–S7, Supporting Information) on blend films with and without 2% GxI additives, to check whether or not there is significant change in the film morphology or EQE at the GxI absorption. These measurements do not show any considerable change in film morphology upon adding GxI. Also, if there were morphological differences, we would have observed changes in the geminate recombination loss,[40] followed by reduction in PL quenching, as reported by Liedtke et al.[37] In contrast, we have not seen any PL enhancement in the blend

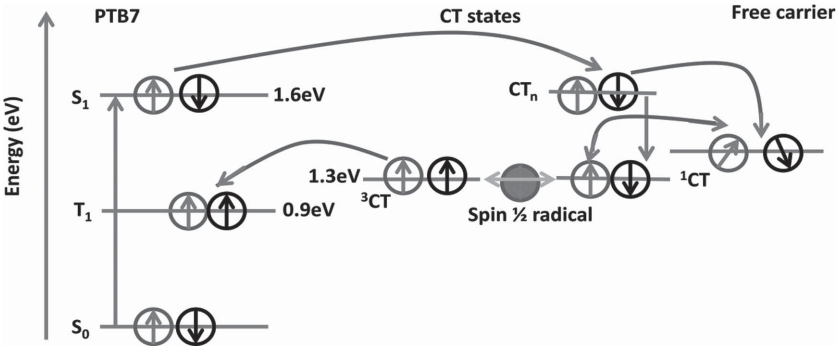

Figure 5. Schematic of the charge transfer processes in the PTB7/C60-PCBM blend with GxI radical additives, where the interference of the spin ½ radical with the $^1CT \rightarrow {}^3CT$ intersystem crossing is unraveled.

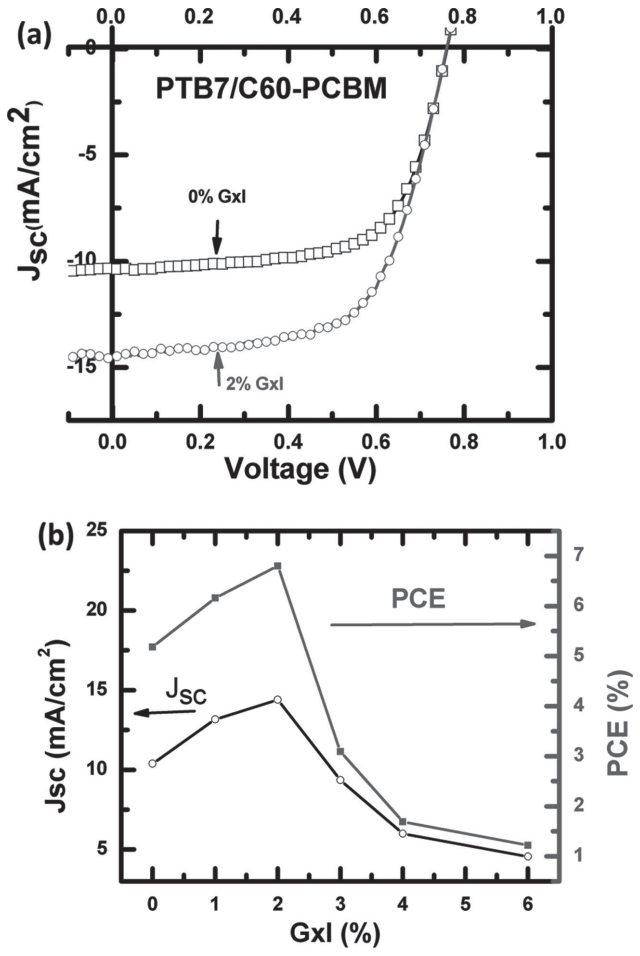

Figure 6. Photovoltaic characteristics of PTB7/C60-PCBM solar cell under AM1.5 sun illumination. a) *I–V* plot of the device without (squares) and with (circles) galvinoxyl additives. b) PCE (squares) and J_{sc} (circles) of the OPV devices versus percentage weight of galvinoxyl.

with Gxl additives; the PL emission intensity does not change upon Gxl additives in the blends (Figure S2b, Supporting Information). Also, the polymer PL spectrum with and without Gxl shows the same 0–0 to 0–1 ratio (Figure S2a, Supporting Information); which indicates that the polymer packing order is unchanged upon Gxl addition. We therefore, conclude that the Gxl additives up to 2%, do not impact the film morphology. In addition, J_{sc} increase upon Gxl additives is not due to the absorption difference in the blends, as shown in absorption and EQE spectra (Figure S1, S4, respectively). In particular, there is no EQE enhancement from the absorption due to Gxl; EQE simply rigidly increases upon Gxl additives throughout the whole spectrum.

Table 1. OPV solar cell device parameters versus galvinoxyl additives' percentage weight.

% Gxl	J_{sc} [mA cm^{-2}]	V_{oc} [V]	FF [%]	PCE [%]
0	10.4	0.77	65	5.2
1	13.2	0.76	62	6.2
2	14.4	0.76	62	6.8
3	9.4	0.72	46	3.1
4	6.0	0.65	43	1.7
6	4.6	0.64	42	1.2

We also studied the Gxl effect in PTB7/C70-PCBM devices, and found that the additives are in fact detrimental to the device performance. **Figure 7**a shows the *I–V* characteristics of the device based on pristine PTB7/C70-PCBM blend and the same blend doped with 2% weight Gxl. In contrast to the case of PTB7/C60-PCBM blend discussed above, where adding Gxl improves the device performance, the device performance here decreases after adding 2% Gxl. PCE decreases from 6.8% (J_{sc} = 18.7 mA cm^{-2}, V_{oc} = 0.70 V, FF = 0.52) to 3.7% (J_{sc} = 11.0 mA cm^{-2}, V_{oc} = 0.69 V, FF = 0.49). It is clear that the decrease in PCE is mainly due to a decrease in J_{sc}. According to the scheme proposed above, Gxl is unable to decrease the major loss mechanism due to the back reaction CT→TE in the copolymer. This may be explained due to a different CT energy level at the PTB7/C70-PCBM interface compared with that at the PTB7/C60-PCBM interface, which is no longer in resonance with the Gxl spin ½ SOMO level, or due to faster dissociation rate of ^{1}CT compared with the CT→TE reaction rate, or both.[25] In this case, the Gxl additives may act as defects and hinders carrier transport, which also reduces J_{sc} in the OPV device. In order to unravel the underlying mechanism for the inferior performance in devices based on the PTB7/C70-PCBM with Gxl additives, we performed cw and transient PA measurements.

The PA spectra of PTB7/C70-PCBM undoped and Gxl-doped blends are shown in Figure 7b. Similar to the PTB7/C60-PCBM blend, they show the PA at 0.4 eV due to P_1 of polarons and another PA band at 1.1 eV that has contributions from both polaron P_2 band and triplet PA. In contrast to the PA spectra of PTB7/C60-PCBM however, there is not much difference in the PA spectra of PTB7/C70-PCBM undoped and Gxl-doped blends. Also the MPA(*B*) response at 1.1 eV (Figure 7c) is still dominated by the response of TE even after Gxl doping. Moreover, the ultrafast transient PA(*t*) at 1.1 eV of the PTB7/C70-PCBM undoped and Gxl doped blends also do not change much upon Gxl doping (Figure 7d). These results imply that the Gxl radical is unable to reduce the TE formation in this blend. Still, it may be possible to find other spin ½ radicals, which match the CT energy in this blend, and thus would suppress the CT→TE back reaction and consequently increase the formation of free carriers. It is noteworthy that the CT→TE loss is not substantive in the undoped PTB7/C70-PCBM blend. This can be seen from the ps transient PA(*t*) results (Figure 7d); the increase in the PA at 1.1 eV is not as large as that in PTB7/C60-PCBM (Figure 4d). This may explain the relatively higher PCE of OPV cells based on this blend (6.8%; Figure 7a) compared with the low PCE in devices based on PTB7/C60-PCBM (5.2%; Figure 6a).

3. Conclusion

We studied the optical, electrical, and magnetic properties of films and devices based on the low bandgap copolymer PTB7 donors and its blends with C60-PCBM and C70-PCBM acceptors. We identified the PA band of TE in the pristine

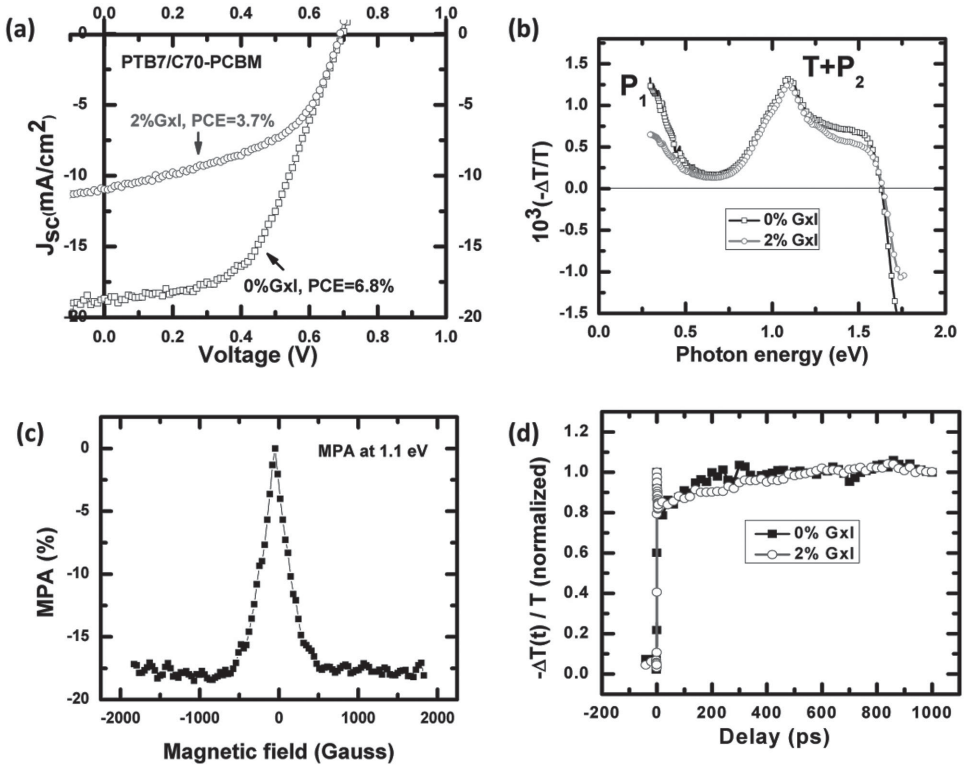

Figure 7. Photovoltaic device characteristics and photophysics of films based on PTB7/C70-PCBM. a) Photocurrent *I–V* under AM1.5 sun illumination without (squares) and with (circles) galvinoxyl radical additives. b) PA spectrum without (squares) and with (circles) galvinoxyl radical additives. The PA bands P_1 and P_2 + T are denoted. c) MPA(*B*) response of film of PTB7/C70-PCBM blend with GxI additives at 1.1 eV. d) Picosecond transient PA(*t*) at 1.1 eV of the blend film without (squares) and with (circles) galvinoxyl additives.

copolymer that occurs at 1.1 eV and polaron absorption bands at 0.4 and 1.1 eV, respectively using the cw techniques of DIA, PADMR, and MPA. We unraveled a loss mechanism that reduces the photocurrent in PTB7-based devices as the back reaction CT→TE in the copolymer chains. We clearly see that this loss process is dramatically reduced by adding a few percentage of the spin ½ GxI radicals. This leads to substantial enhancement of OPV device performance based on PTB7/C60-PCBM blend, of up to 30% increase in PCE. However, devices based on PTB7/C70-PCBM blend do not show improvement upon GxI doping. We showed that the GxI inability to improve the device performance in PTB7/C70-PCBM blend is related to its inability to suppress the back reaction CT→TE. This work provides a new avenue for improving the PCE of OPV devices based on LBG copolymers by adding spin ½ radicals, which may be performed in addition to other, more traditional methods.

4. Experimental Section

The PTB7 polymer was synthesized as described elsewhere;[10] C60-PCBM and C70-PCBM were purchased from American Dye Source, Inc., Canada; and GxI was purchased from Sigma-Aldrich, USA. These materials were used "as received" without further purification. The polymer solution is prepared in 1,2-dichlorobenzene (ODCB) solvent at a concentration of 10 mg mL^{-1}. PTB7/PCBM blend films were prepared in the ratio of 1:1.5 by weight in a mixture of two solvents: ODCB and 1,8- diiodooctane (DIO), at a ratio of 97:3 by volume. Several percentage weights of GxI radicals were mixed in the blend solution for studying the effect of spin½ radical additives on the OPV cell performance versus GxI concentration. Spin-coated films were used for both optical and electrical studies.

For the PA and photoluminescence (PL) spectroscopies, we placed the films in a closed cycle He refrigerator cryostat at 50 K. The steady state PA spectrum was measured using a standard setup.[14] We used for the pump excitation a diode laser at $\hbar\omega = 1.8$ eV that was modulated at frequency, *f* of 310 Hz; whereas the output beam of an incandescent tungsten/halogen lamp was used as a probe light source. The change, ΔT in the probe transmission, *T* induced by the laser pump excitation was measured by several solid state detectors in the probe range of 0.25–2.5 eV, and the PA spectrum was obtained from the relation PA = $-\Delta T/T$ (the negative fractional change in transmission). The ultrafast transient PA dynamics was performed in another PA setup described in details found in the literature.[15] For these measurements, we used the pump/probe correlation technique in the mid-IR spectral range with 150 fs time resolution, where the time, *t* was set by a translation stage.

The same cw PA setup was used for the MPA measurements, with an external magnetic field provided by an electromagnet that produced field, *B* up to 1800 Gauss that was applied parallel to the film surface. The MPA(*B*) response is defined by the relation MPA(*B*) = [PA(*B*)–PA(0)]/PA(0), where PA(*B*) is the PA at field strength *B*, and PA(0) is the PA at $B = 0$.[32] For the PADMR measurements, we used an optically accessed 3 GHz μ-wave resonator located between the poles of a superconducting electromagnet inside the Helium-cooled cryostat as described in detail elsewhere.[42]

The OPV device structure was fabricated in the form of ITO/HTL/active layer/Ca/Al. HTL, or hole transport layer, consisted of a 40-nm thick film of PEDOT:PSS poly(3,4-ethylenedioxythiophene)/poly(styrenesulfonate); the active layer was a ≈100-nm thick film of PTB7/fullerene

blend; and the cathode was a calcium thin film (20-nm thick) capped with an aluminum layer for protection; the device area was 2 mm × 2 mm. *I–V* characteristics were measured using a Xenon lamp light source (calibrated with Si PV purchased from NREL) using a Keithley 236 Source-Measure unit under AM1.5 illumination conditions in an encapsulated device.

Supporting Information

Supporting Information is available from the Wiley Online Library or from the author.

Acknowledgements

The authors thank Ryan McLaughlin for fruitful discussions. The work of T.B., the OPV device investigation, and cw spectroscopies were supported by the NSF-MRSEC program at the University of Utah, Grant No. DMR 1121252. The work of U.H. and the ps spectroscopy were supported by the DOE Grant No. DE-FG02–04ER46109 at the University of Utah. Partial supports from NSF and AFOSR to LPY are appreciated.

Received: September 14, 2014
Revised: January 6, 2015
Published online: February 18, 2015

[1] C. W. Tang, *Appl. Phys. Lett.* **1986**, *48*, 183.
[2] J.-H. Huang, J.-H. Fang, C.-C. Liu, C.-W. Chu, *ACS Nano* **2011**, *5*, 6262.
[3] J. You, L. Dou, K. Yoshimura, T. Kato, K. Ohya, T. Moriarty, K. Emery, C.-C. Chen, J. Gao, G. Li, *Nat. Commun.* **2013**, *4*, 1446.
[4] F. C. Krebs, N. Espinosa, M. Hösel, R. R. Søndergaard, M. Jørgensen, *Adv. Mater.* **2014**, *26*, 29.
[5] D. Venkataraman, S. Yurt, B. H. Venkatraman, N. Gavvalapalli, *J. Phys. Chem. Lett.* **2010**, *1*, 947.
[6] G. Li, R. Zhu, Y. Yang, *Nat. Photonics* **2012**, *6*, 153.
[7] Y. Liang, Z. Xu, J. Xia, S. T. Tsai, Y. Wu, G. Li, C. Ray, L. Yu, *Adv. Mater.* **2010**, *22*, E135.
[8] G. Yu, J. Gao, J. Hummelen, F. Wudl, A. Heeger, *Science* **1995**, *270*, 1789.
[9] M. Morana, H. Azimi, G. Dennler, H. J. Egelhaaf, M. Scharber, K. Forberich, J. Hauch, R. Gaudiana, D. Waller, Z. Zhu, *Adv. Funct. Mater.* **2010**, *20*, 1180.
[10] Y. Liang, L. Yu, *Acc. Chem. Res.* **2010**, *43*, 1227.
[11] G. Li, V. Shrotriya, J. Huang, Y. Yao, T. Moriarty, K. Emery, Y. Yang, *Nat. Mater.* **2005**, *4*, 864.
[12] F. Gao, O. Inganäs, *Phys. Chem. Chem. Phys.* **2014**, *16*, 20291.
[13] E. W. Snedden, A. P. Monkman, F. B. Dias, *J. Phys. Chem. C* **2012**, *116*, 4390.
[14] G. Hukic-Markosian, T. Basel, S. Singh, Z. V. Vardeny, S. Li, D. Laird, *Appl. Phys. Lett.* **2012**, *100*, 213903.
[15] S. Singh, B. Pandit, T. P. Basel, S. Li, D. Laird, Z. V. Vardeny, *Phys. Rev. B* **2012**, *85*, 205206.
[16] A. A. Bakulin, A. Rao, V. G. Pavelyev, P. H. van Loosdrecht, M. S. Pshenichnikov, D. Niedzialek, J. Cornil, D. Beljonne, R. H. Friend, *Science* **2012**, *335*, 1340.
[17] L. Dou, C.-C. Chen, K. Yoshimura, K. Ohya, W.-H. Chang, J. Gao, Y. Liu, E. Richard, Y. Yang, *Macromolecules* **2013**, *46*, 3384.
[18] Y. Zhu, R. D. Champion, S. A. Jenekhe, *Macromolecules* **2006**, *39*, 8712.
[19] Y. Zhang, T. P. Basel, B. R. Gautam, X. Yang, D. J. Mascaro, F. Liu, Z. V. Vardeny, *Nat. Commun.* **2012**, *3*, 1043.
[20] J. H. Seo, A. Gutacker, Y. Sun, H. Wu, F. Huang, Y. Cao, U. Scherf, A. J. Heeger, G. C. Bazan, *J. Am. Chem. Soc.* **2011**, *133*, 8416.
[21] R. Noriega, J. Rivnay, K. Vandewal, F. P. Koch, N. Stingelin, P. Smith, M. F. Toney, A. Salleo, *Nat. Mater.* **2013**, *12*, 1038.
[22] J. Gilot, M. M. Wienk, R. A. Janssen, *Adv. Mater.* **2010**, *22*, E67.
[23] M. Reyes-Reyes, K. Kim, D. L. Carroll, *Appl. Phys. Lett.* **2005**, *87*, 083506.
[24] R. Tautz, E. Da Como, T. Limmer, J. Feldmann, H.-J. Egelhaaf, E. Von Hauff, V. Lemaur, D. Beljonne, S. Yilmaz, I. Dumsch, *Nat. Commun.* **2012**, *3*, 970.
[25] A. Rao, P. C. Chow, S. Gélinas, C. W. Schlenker, C.-Z. Li, H.-L. Yip, A. K.-Y. Jen, D. S. Ginger, R. H. Friend, *Nature* **2013**, *500*, 435.
[26] A. E. Jailaubekov, A. P. Willard, J. R. Tritsch, W.-L. Chan, N. Sai, R. Gearba, L. G. Kaake, K. J. Williams, K. Leung, P. J. Rossky, *Nat. Mater.* **2013**, *12*, 66.
[27] C. Piliego, M. A. Loi, *J. Mater. Chem.* **2012**, *22*, 4141.
[28] M. K. Etherington, J. Wang, P. C. Chow, N. C. Greenham, *Appl. Phys. Lett.* **2014**, *104*, 063304.
[29] J. M. Szarko, B. S. Rolczynski, S. J. Lou, T. Xu, J. Strzalka, T. J. Marks, L. Yu, L. X. Chen, *Adv. Funct. Mater.* **2014**, *24*, 10.
[30] K. M. Noone, S. Subramaniyan, Q. Zhang, G. Cao, S. A. Jenekhe, D. S. Ginger, *J. Phys. Chem. C* **2011**, *115*, 24403.
[31] R. Österbacka, C. An, X. Jiang, Z. Vardeny, *Science* **2000**, *287*, 839.
[32] B. R. Gautam, T. D. Nguyen, E. Ehrenfreund, Z. V. Vardeny, *Phys. Rev. B* **2012**, *85*, 205207.
[33] T. Basel, *PhD Thesis*, The University of Utah **2014**.
[34] T. Drori, E. Gershman, C. Sheng, Y. Eichen, Z. V. Vardeny, E. Ehrenfreund, *Phys. Rev. B* **2007**, *76*, 033203.
[35] M. R. Hammond, R. J. Kline, A. A. Herzing, L. J. Richter, D. S. Germack, H.-W. Ro, C. L. Soles, D. A. Fischer, T. Xu, L. Yu, *ACS Nano* **2011**, *5*, 8248.
[36] S. J. Lou, J. M. Szarko, T. Xu, L. Yu, T. J. Marks, L. X. Chen, *J. Am. Chem. Soc.* **2011**, *133*, 20661.
[37] M. Liedtke, A. Sperlich, H. Kraus, A. Baumann, C. Deibel, M. J. Wirix, J. Loos, C. M. Cardona, V. Dyakonov, *J. Am. Chem. Soc.* **2011**, *133*, 9088.
[38] B. A. Collins, Z. Li, J. R. Tumbleston, E. Gann, C. R. McNeill, H. Ade, *Adv. Energy Mater.* **2013**, *3*, 65.
[39] S. Ochiai, S. Imamura, S. Kannappan, K. Palanisamy, P.-K. Shin, *Curr. Appl. Phys.* **2013**, *13*, S58.
[40] A. Foertig, J. Kniepert, M. Gluecker, T. Brenner, V. Dyakonov, D. Neher, C. Deibel, *Adv. Funct. Mater.* **2014**, *24*, 1306.
[41] S. Guo, E. M. Herzig, A. Naumann, G. Tainter, J. Perlich, P. Müller-Buschbaum, *The J. Phys. Chem. B* **2013**, *118*, 344.
[42] C. Yang, E. Ehrenfreund, Z. Vardeny, *Phys. Rev. Lett.* **2007**, *99*, 157401.